Surface-Plasmon Quantum Cascade Microlasers with Highly-Deformed Resonators

R. Colombelli[1], C. Gmachl[2], A. M. Sergent[3], D. L. Sivco[3], E. Narimanov[2], V. Podolskiy[4], A. Y. Cho[3], and F. Capasso[5]

[1] *Institut d'Electronique Fondamentale - Bât. 220, Université Paris-Sud, 91405 Orsay, FRANCE*
[2] *Department of Electrical Engineering and PRISM, Princeton University, Princeton, NJ 08544, USA*
[3] *Bell Laboratories, Lucent Technologies, Murray Hill, NJ 07974, USA*
[4] *Physics Department, 301 Weniger Hall, Oregon State University, Corvallis, OR 97331*
[5] *Division of Engineering and Applied Sciences, Harvard University, Cambridge, MA 02138, USA*

Abstract

We report the demonstration of surface-plasmon micro-cylinder Quantum Cascade lasers with circular and deformed resonators. An improved, self-alignment fabrication technique was developed that allows the use of wet etching, necessary to achieve smooth and clean surfaces, in combination with the deposition of the surface-plasmon carrying metal layer up to the very edge of the resonator, where the optical mode is mostly located. The diameter of the micro-cylinders ranges from 75 μm to 180 μm while their deformation coefficient ε ranges from ε=0 to ε= 0.32). Circular micro-cylinder lasers show a reduction of ~ 50 % of the threshold current density with respect to devices with standard ridge-waveguide resonators. On the other hand, highly deformed micro-cylinder lasers exhibit a complex mode structure, suggesting the onset of chaotic behavior.

Index Terms—Mid-infrared, unipolar devices, micro-disks lasers, micro-lasers

Recent advances in the development of Quantum Cascade (QC) lasers [1] dramatically extended their operating wavelengths well into the far-infrared and THz ranges [2]. This success was prompted not only by the use of advanced quantum designs, but also by the innovative use of waveguides based on surface plasmon polaritons, originally demonstrated in the mid-infrared [3]. The availability of very long wavelengths makes the development of QC lasers using micro-disk or micro-cylinder resonators especially interesting. The prospect of very low current thresholds and single mode emission is a result of the miniaturized dimension of the cavity and the intrinsically low out-coupling losses, due to the advantageous ratio between the length-scale of the sidewalls roughness and the operating wavelength. Rayleigh scattering of the light at the sidewalls is reduced, with beneficial effects on the threshold current density. As for the output power, it was shown by Gmachl et al. [Ref. 13] that it can be increased by even 3 orders of magnitude if a clever deformation is added to the cavity shape. In fact – for a limited range of deformations – so called "bowtie" modes exist that exhibit a high *Q* factor and at the same time can more easily escape thanks to refractive effects. Finally, the longer wavelength allows to achieve high Q/V_{eff} factors without fabricating prohibitive small cavities, where Q is the quality factor of the cavity, and V_{eff} is the effective mode volume.

In surface-plasmon based QC lasers the optical mode is a TM polarized electromagnetic wave bound at the top metal-semiconductor interface, that decays exponentially away from the latter. The top metal is therefore an essential part of the waveguide. Since whispering gallery (WG) optical modes are located mostly at the periphery of the disc [4], it is essential that the top metal contact - and thus the waveguide - extends to the very edge of the micro-cylinders. It is possible to fulfill this requirement when the top contact is used as a metallic mask and the semiconductor is etched *via* reactive ion etching. However, the use of dry- instead of wet-etching techniques constitutes a serious drawback since the surface roughness is more pronounced and the achievable *Q*-factors are smaller.

In this paper we report the demonstration of surface-plasmon micro-cylinder QC lasers. The devices have been realized with an improved fabrication technique that allows to combine the advantages of wet etching with the requirement of a metal contact/waveguide extending to the edge of the resonator.

The laser structures have been grown by molecular-beam epitaxy using $In_{0.53}Al_{0.47}As/Al_{0.48}In_{0.52}As$ lattice matched to a low-doped ($n \approx 2x10^{17}$ cm^{-3}) InP substrate. The active regions of the lasers are based on interminiband transitions in "chirped" undoped

superlattices. They have been designed for the longest possible emission wavelengths compatible with the InGaAs/AlInAs material system, i.e. $\lambda \approx 17$, 19, 21 and 24 μm [5-8]. The details of the growth are reported in Ref. [5-8]. Seventy-five active region/injector stages were grown for the $\lambda = 17$, 21 and 24 μm lasers, while only forty stages were grown for the $\lambda = 19$ μm laser [7].

The fabrication procedure is described in Fig. 1. The core improvement consists in using a double-layer mask (SiN and resist) in order to avoid a second lithography after the semiconductor etch and before the evaporation of the top metallic contacts. Such second lithography would not allow to perfectly match the shape of the etched micro-cylinders, due to unavoidable undercut effects and to limits to the achievable alignment precision. After the deposition of a 300-nm-thick SiN layer, resist is patterned with optical lithography (Fig. 1a,b). The patterns (circular or stadium-shaped) are then transferred to the SiN with reactive ion etching (Fig. 1c), and the SiN-resist double-layer is used as a mask for the semiconductor wet etch (Fig. 1d). The resist is then removed with a solvent (Fig. 1e) and then deposited again through spin-coating. Thanks to the sharp undercut of the SiN layer and to the surface adhesion forces, the resist assumes an unusual shape (see Fig. 1f and Fig.2): it partially covers the top surface of the SiN mask, but it completely fills the space left by the undercut. Dipping the sample in HF acts as “lift-off”, etching away the sacrificial SiN layer, and leaving the micro-cylinders surfaces exposed, while the rest of the sample is still covered by resist. A top metal contact (Ti/Au, 100 Å/2000 Å) is then evaporated, followed by a lift-off in acetone (Figs. 1h,i). The results are shown in Fig.3. Particularly Fig. 3b proves that the metal, and therefore the waveguide, covers the whole surface of the resonator.

After polishing and back-contact deposition, the samples were soldered with indium to a copper block and mounted in a cryogenically cooled micro-positioner stage, where each device could be contacted individually with a microprobe. While all the lasers could operate in pulse mode, only the 19 μm laser achieved continuous wave (CW) operation. In this paper we will concentrate on this latter set of devices.

Fig. 4a shows some selected laser spectra for an almost circular device operated at 10 K in CW. The threshold current density for this device was ≈ 1.5 kA/cm^2. This value should be compared to the value of 3.2 kA/cm^2, obtained from the same material processed as standard Fabry-Perot ridge resonators[Ref. 7]. The resonator length was in that case 375 μm, which gives rise to high out-coupling losses. The dramatic reduction of the threshold current density - about 50 % - is likely caused by two factors. In micro-cylinder lasers the light circulates in the outer part of the disc. Since the light is confined by total internal reflection, there are only

minute losses caused by evanescent leakage and scattering from surface roughness. This allows one to reduce the device dimensions – with beneficial effects on the heat dissipation for CW operation – without dramatically increasing the out-coupling losses. In addition, our fabrication technique is a one-step process. No SiN is deposited on the sidewalls for insulation, and no additional lithography is required after the semiconductor etch, thereby keeping the surface-roughness and sidewalls deterioration to a minimum. The *Q*-factor of our resonator can be estimated in a straightforward manner. We can infer the out-coupling losses from the following expression for the threshold current density [9]: $J_{th} = \frac{\alpha_w + \alpha_{out}}{g\Gamma}$, where α_w = 62 cm^{-1} are the material losses, α_{out} are the out-coupling losses, Γ = 0.81 is the mode confinement factor, and *g* is the material gain. Using the calculated values for *g* (=58 cm/kA) and Γ (=0.81) [6], and the experimental value for J_{th} (=1.5 kA/cm^2), we obtain ($\alpha_w + \alpha_{out}$) ≈ 70 cm^{-1}. In turn, this corresponds to $Q \approx 300$, using the following formula: $Q = \frac{2\pi \cdot n_{eff}}{\lambda \cdot (\alpha_w + \alpha_{out})}$ [9]. Since $\alpha_w \approx 62$ cm^{-1}, the *Q*-factor of our resonator is mainly limited by the material losses. However, Q ≈ 300 is a relatively high value for a $\lambda \approx 19$ μm laser [9], and it suggests that this approach is potentially very interesting in the THz range. As a matter of fact, in that wavelength range material losses have been shown to be ≈ 6-8 cm^{-1}. Even lower values, between 0.5 and 1 cm^{-1}, can be achieved when the device is operated in presence of a magnetic field [10].

Recent theoretical work [11] suggested that effects known from the field of nonlinear dynamics, such as *chaos-assisted tunneling*, could arise in highly deformed micro-resonators. The magnitude of these effects, that can reveal themselves as minute splittings of the laser lines for increased deformations, scales with the emission wavelength as λ/r, where *r* is the average radius of the micro-resonator [11]. In addition, the deformation should be quadrupolar ($r(\varphi) \propto [1 + \varepsilon \cdot \cos(2\varphi)]$), or "flattened" quadrupolar ($r(\varphi) \propto [1 + \varepsilon \cdot \cos(2\varphi)]^{1/2}$) shape [12] or an equivalent shape. Such a shape can be obtained with wet etching, starting from a stadium-shape resist pattern (i.e. two semicircles connected by a rectangle). Thanks to the smoothing action of the etchant, the straight sections gradually bend toward the curved parts, eventually rendering a (flattened) quadrupole shape [12]. It is worth it to note that the (flattened) quadrupolar shape is difficult to obtain without wet etching, since it would require the use of a very high resolution laser (or even electron-beam) stepper.

We fabricated surface-plasmon QC micro-cylinder lasers with a flattened quadrupolar shape and several different deformation values (ranging from ε = 0 to ε = 0.32 using the λ =

19 μm material. The choice of the λ = 19 μm laser was motivated by its ability to operate in CW mode. Unwanted effects such as frequency chirping were therefore avoided, as well as the onset of transverse modes. On the contrary, these effects heavily affected the other lasers that could operate in pulsed mode only (see Fig. 4c).

Fig. 5 shows the mode chart (emission wavelength *vs* injected current) for several devices with different deformations. Except for a limited and initial current range, lasers are usually multimode. .

While for small deformations (ε<0.1) the mode distribution can be roughly explained with a ray-optics approach, for high deformations several additional modes suddenly appear. On one hand, the complexity of the spectrum is real, since the lasers operate in CW. The exceptional number of modes observed cannot therefore be attributed - for instance - to changes of n_{eff} during time, since the devices are in steady state. On the other hand, the number and distribution of the observed modes could not conclusively be attributed to *chaos-assisted tunneling* effects. A third hypothesis invokes spatial inhomogeneity: different modes could have spatial distributions that do not overlap. However, we observed mode-competition effects in some highly-deformed devices, suggesting that the laser modes do actually spatially overlap.

We did not observe a monotonic increase in output power as a function of deformation, as reported in Ref.[13]. Instead, once a deformation was introduced, the power increased by a factor 10 to 90 (depending on the device set) with respect to an exactly circular device, and no trend was observed with deformation. The increase in output power observed in Ref. [13] is related to the onset of the *bowtie* mode, and to the fact that with the given effective index of refraction strong outcoupling of light occurs, as the condition for total internal reflection is met at angles very close to the bounce angles of the bow-tie modes. In the devices discussed here, we believe that we did not excite the bow-tie modes. We propose two explanations for that.

Our fabrication technique allowed to deposit metal up to the very edge of the disk (see Fig. 3), contrary to what is usually the case for mid-IR micro-disk QC lasers [4,13], where the contact covers the center of the resonator only. The latter configuration might be more suited to excite a *bowtie* mode, since it preferentially pumps the center of the disk, introducing a clear competitive disadvantage for the WG modes, that are mostly located on the periphery of the disk. In our case instead, the current is injected uniformly on all the surface of the cavity: WG and *bowtie* modes now compete on equal grounds. The higher *Q*-factors due to the longer wavelength (and especially the lower out-coupling losses) may have shifted the

advantage from the *bowtie* to the WG modes. Secondly, the surface-plasmon modes have generally a larger effective refractive index; as a result, the angle of total internal reflection is smaller that in Ref. 13, and as a result the bow-tie modes are more lossy, and are less likely to be excited.

In conclusion, we demonstrated pulsed and CW-operating micro-cylinder quantum cascade lasers with surface plasmon waveguides at very long wavelengths ($\lambda \approx 17$ to 24 μm). An improved fabrication technique was developed that not only allows the fabrication of the devices with wet-etching, but it also succeeds in achieving microcavities with high *Q*-factors. Results on highly deformed micro-resonators show anomalous spectral behaviors that – to date – could not be explained even by considering the onset of chaotic effects. In fact, the onset of a complex spectral behavior with increasing deformations may suggest that *quantum chaos* phenomena are becoming manifest. In order to exclude any effect related to spatial inhomogeneities, angle resolved measurements could be performed. This technique might allow one to infer the mode spatial distribution.

ACKNOWLEDGMENT

This material is based upon work supported in part by DARPA/ARO under Contract No. DAAD19-00-C-0096. We acknowledge useful discussions and help from Milton L. Peabody, Mariano Troccoli, Alex Soibel. Federico Capasso acknowledges partial financial support from the Airforce Office of Scientific Research under contract MURI FA 9550-04-1-0434. Raffaele Colombelli acknowledges support from the European Science Foundation, through the EURYI "Young Investigator Award" program.

REFERENCES

[1] F. Capasso, R. Paiella, R. Martini, R. Colombelli, C. Gmachl, T. L. Myers, M. S. Taubman, R. M. Williams, C. G. Bethea, K. Unterrainer, H. Y. Hwang, D. L. Sivco, A. Y. Cho, A. M. Sergent, H. C. Liu, and E. A. Whittaker, "*Quantum Cascade Lasers: Ultrahigh-Speed Operation, Optical Wireless Communication, Narrow Linewidth and Far-Infrared Emission*", IEEE J. Quantum Electron. **38**, 511 (2002), and references therein.

[2] R. Köhler, A Tredicucci, F. Beltram, H. E. Beere, E. H. Linfield, A. G. Davies, D. A. Ritchie, R. C. Iotti, and F. Rossi, "*Terahertz semiconductor heterostructure laser*", Nature **417**, 156 (2002); S. Kumar, B. S. Williams, S. Kohen, and Q. Hu, "*Continuous-wave operation of terahertz quantum-cascade lasers above liquid-nitrogen temperature*",Appl. Phys. Lett. **84**, 2494 (2004);

G. Scalari, L.Ajili, J. Faist, H. Beere, E. Linfield, D. Ritchie, and G. Davies , "*Far-infrared (λ=87 μm). bound-to-continuum quantum-cascade lasers operating up to 90 K*", Appl. Phys. Lett. **82**, 3165 (2003).

[3] C. Sirtori, C. Gmachl, F. Capasso, J. Faist, D. L. Sivco, A. L. Hutchinson, and A. Y. Cho, "*Long-wavelength (l ø 8–11.5 mm) semiconductor lasers with waveguides based on surface plasmons"***,** Opt. Lett. **23**, 1366 (1998).

[4] J. Faist, C. Gmachl, M. Striccoli, C. Sirtori, F. Capasso, D. L. Sivco, and A. Y. Cho, "*Quantum cascade disk lasers"*, Appl. Phys. Lett. **69,** 2456 (1996).

[5] A. Tredicucci, C. Gmachl, F. Capasso, A. L. Hutchinson, D. L. Sivco, and A. Y. Cho, "*Long wavelength superlattice quantum cascade lasers at λ=17 μm*", Appl. Phys. Lett. **74** 638 (1999).

[6] A. Tredicucci, C. Gmachl, M. C. Wanke, F. Capasso, A. L. Hutchinson, D. L. Sivco, S.N. G. Chu, and A. Y. Cho, "*Surface plasmon quantum cascade lasers at λ=19 μm*"Appl. Phys. Lett. **77** 2286 (2000).

[7] R. Colombelli, A. Tredicucci, C. Gmachl, F. Capasso, D.L. Sivco, A.M. Sergent, A.L. Hutchinson, and A.Y. Cho, "*Continuous Wave Operation of λ = 19 μm Surface-Plasmon Quantum Cascade Lasers*", El. Lett. **37**, 1023 (2001).

[8] R. Colombelli, F. Capasso, C. Gmachl, A. L. Hutchinson, D. L. Sivco, A. Tredicucci, M. C. Wanke, A. M. Sergent, and A. Y. Cho, "*Far-infrared Surface-Plasmon Quantum-Cascade Lasers at 21.5 μm and 24 μm Wavelengths*", Appl. Phys. Lett. **78**, 2620 (2001).

[9] C. Gmachl, F. Capasso, D. L. Sivco, and A. Y. Cho, "*Recent progress in quantum cascade lasers and applications*", Rep. Prog. Phys. **64**, 1533 (2001).

[10] L. Ajili, G.Scalari, J.Faist, H. Beere, E.Linfield, D.Ritchie, G.Davies, "*High power quantum cascade lasers operating at λ=87 and 130 μm*", Appl. Phys. Lett. **85**, 3986 (2004); G. Scalari, S. Blaser, J. Faist, H. Beere, E. Linfield, D. Ritchie, and G. Davies, "*Terahertz Emission from Quantum Cascade Lasers in the Quantum Hall Regime: Evidence for Many Body Resonances and Localization Effects*", Phys. Rev. Lett. **93** 237403 (2004).

[11] V. A. Podolskiy, and E. E. Narimanov, "*Semiclassical description of chaos-assisted tunneling"*, Phys. Rev. Lett. **91**, 263601 (2003); V. A. Podolskiy, and E. E. Narimanov, "*Chaos-assisted tunneling in whispering-gallery resonators*", Proc. SPIE Int. Soc. Opt. Eng. **4969**, 167 (2003).

[12] C. Gmachl, F. Capasso, E. E. Narimanov, J. U. Nockel, A. D. Stone, J. Faist, D. L. Sivco, and A. Y. Cho, "*High-Power Directional Emission from Microlasers with Chaotic Resonators*", Science **280**, 1556 (1998).

[13] C. Gmachl, E. E. Narimanov, F. Capasso, J. N. Baillargeon, and A. Y. Cho, "*Kolmogorov–Arnold–Moser transition and laser action on scar modes in semiconductor diode lasers with deformed resonators*",Opt. Lett. **27**, 824 (2002).

CAPTIONS

Fig. 1: Fabrication steps of the surface-plasmons micro-disk QC lasers. (a) SiN and resist deposition. (b) Optical lithography. (c) Pattern transfer to the SiN with reactive ion etching. (d) Semiconductor wet etch. (e) Resist removal with acetone. (f) Spin coating at high spinner rotation speeds. (g) HF *lift-off*. (h) Top metal contact evaporation. (i) Acetone lift-off.

Fig. 2: Optical microscope image of a sample that was cleaved after the second resist deposition. The unusual shape of the resist is due – as stated in the text – to the semiconductor undercut in combination with the resist surface adhesion forces. It is worth it to note the exceptional thickness (≈ 10 μm) that the resist achieves in this circumstance.

Fig. 3: (a) Scanning electron microscope (SEM) image of a fabricated device. (b) Top view of a device through an optical microscope. The top metallization extends up to the very edge of the micro-cylinder.

Fig. 4: Selected laser spectra (T=10K) of an almost circular device (with major and minor axis of a=47.5 μm and b = 45 μm, respectively, corresponding to $\varepsilon \approx 0.027$) for different injection currents (linear scale). The device was operated in CW, with injection currents of (right to left) 120, 130, 140, 160, 180, 200 and 220 mA, respectively. (b) A typical spectrum in logarithmic scale, showing a sideband suppression ratio of ~ 25 dB. (c) Typical spectra for the λ = 21 μm laser, operating in pulsed mode, showing the presence of frequency chirping effects.

Fig 5: Mode charts of four devices with different deformations. All the devices were operated in CW, at a temperature of 10 K. (a) $\varepsilon \approx 0.032$ (a=48 μm, b = 45 μm). (b) $\varepsilon = 0.09$. (c) $\varepsilon = 0.17$. (d) $\varepsilon = 0.29$ (a=84 μm, b = 47 μm).
Insets: Optical micro-images of the measured devices, and typical measured spectra.

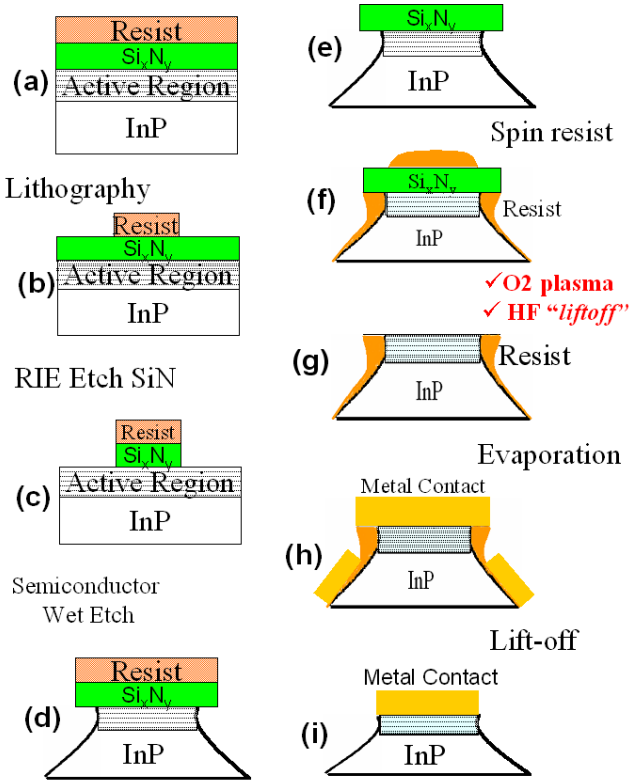

R. Colombelli et al., Fig. 1

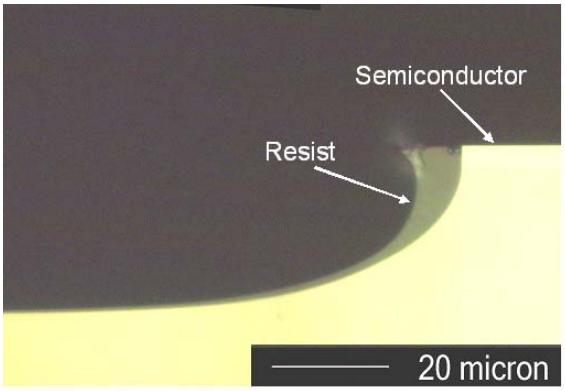

R. Colombelli et al., Fig. 2

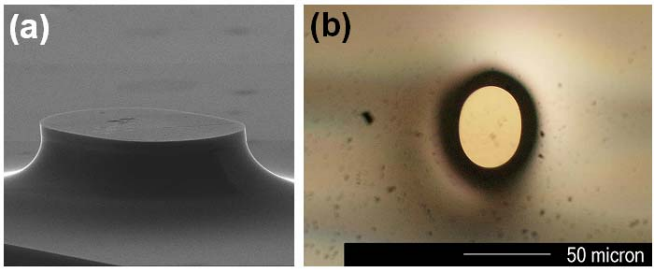

R. Colombelli et al., Fig. 3

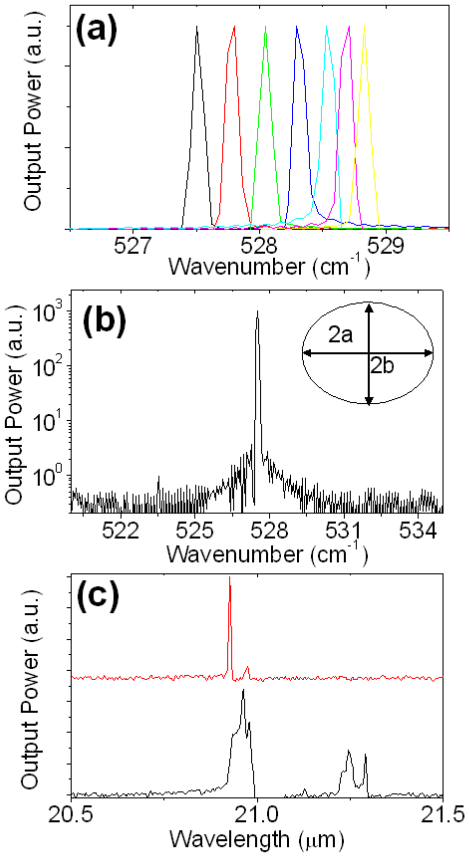

R. Colombelli et al., Fig. 4

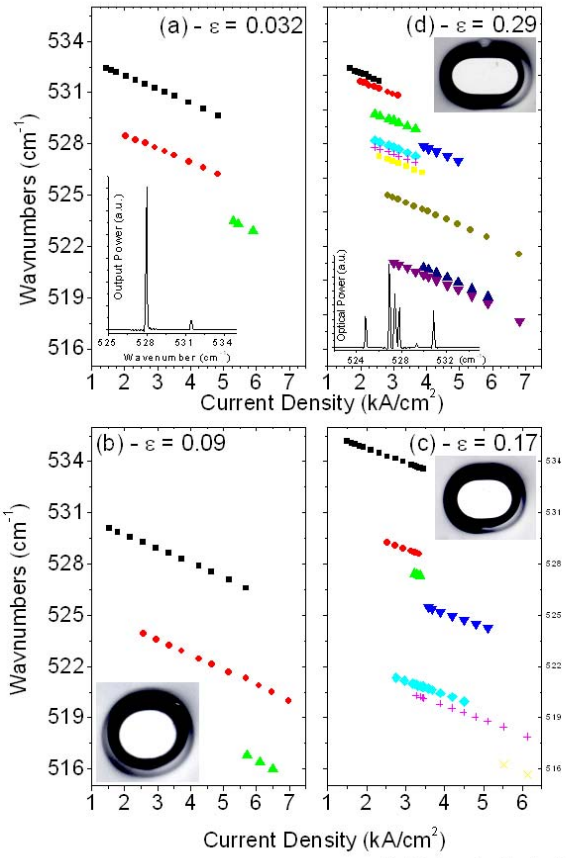

R. Colombelli et al., Fig. 5